Nanoscale

ROYAL SOCIETY OF CHEMISTRY

PAPER

View Article Online
View Journal | View Issue

Cite this: *Nanoscale*, 2021, **13**, 17116

Microscopic origin of near- and far-field contributions to tip-enhanced optical spectra of few-layer MoS_2†

Kathrin Kroth, Philip Klement, Limei Chen, Sangam Chatterjee and Peter J. Klar *

Tip-induced optical spectroscopy overcomes the inherent resolution limits of conventional optical techniques enabling studies of sub-nm sized objects due to the tip's near-field antenna action. This statement is true for individual molecules on surfaces or in the gas phase, but does not hold without restrictions for spatially extended samples. The reason is that the perturbations caused by the tip extend into the sample volume. The tip may induce strain, heating or hot-carrier injection locally in the material. These effects add additional degrees of complexity by changing near-field and far-field optical response. The far-field response varies because strain relaxation, heat and carrier diffusion possess areas of influence exceeding the sample area influenced by the short-range near-field effects. Tip-in spectra are not simply enhanced compared to tip-out spectra, they will also vary in spectral appearance, *i.e.*, peak positions, relative peak intensities, and linewidths. Detailed studies of MoS_2 samples ranging from a single layer to bulk-like multilayer MoS_2 also reveal that the spectra are sensitive to variations of phonon and band structure with increasing layer number. These variations have a direct impact on the signals detected, but also clearly modify the relative magnitudes of the contributions of the tip-induced effects to the tip-in spectra. In addition, the optical response is affected by the kind of tip and substrate used. Hence, the presented results provide further insight into the underlying microscopic mechanisms of tip-enhanced spectroscopy and demonstrate that 2D materials are an ideal playground for obtaining a fundamental understanding of these spectroscopic techniques.

Received 10th May 2021,
Accepted 17th September 2021

DOI: 10.1039/d1nr02987h

rsc.li/nanoscale

1 Introduction

Tip-enhanced Raman spectroscopy (TERS) and tip-enhanced photoluminescence spectroscopy (TEPL) synergize the high spatial resolution of scanning probe microscopy (SPM, such as atomic force microscopy (AFM) or scanning tunnelling microscopy (STM)) and the molecular sensitivity of surface-enhanced Raman spectroscopy (SERS). Here, a metallic, metal-coated or metal-nanoparticle functionalized tip is placed into the laser focus.[1,2] Illumination of the tip excites oscillations of the quasi-free electrons at the apex of the metal tip, so-called localized surface plasmons (LSP). If the laser is in resonance with the LSP wavelength, a strong and localized electromagnetic (EM) near-field will be generated and Raman or photoluminescence (PL) signals in the immediate vicinity of the tip will be significantly enhanced.[1,3] Excited LSP may decay radiatively into photons and non-radiatively into energy-rich electron–hole pairs due to Landau damping.[4] "Hot-carriers" from the metal may be injected into adjacent semiconductors or molecules, if they possess enough energy to overcome the potential barrier between tip and adjacent material.[5] Suitable tips are typically made of Au or Ag, since nanostructures of these noble metals exhibit LSP resonances in the visible range of the electromagnetic spectrum.[1,6] In TERS, enhancement factors are lower in comparison with those typically found in SERS, but nevertheless single molecules may be detected in gap-mode configuration and imaged with sub-nm resolution.[7] Although many technical advances have been made in this research field during the last two decades, the evaluation and the correct interpretation of the tip-enhanced Raman and PL spectra remains challenging in particular in case of ultrathin 2D materials or spatially extended samples. The reason is that the presence of the tip has significant additional impact on the sample other than just the near-field antenna action and hot-carrier injection. The tip may also introduce strain or local heating which will also affect the spectral features of the tip-

I. Physikalisches Institut und Zentrum für Materialforschung (ZfM/LaMa), Justus-Liebig-Universität Giessen, Heinrich-Buff-Ring 16, 35392 Giessen, Germany.
E-mail: Peter.J.Klar@physik.uni-giessen.de

†Electronic supplementary information (ESI) available. See DOI: 10.1039/d1nr02987h

enhanced spectra.[8–13] Even spectral artefacts may occur due to molecules adsorbed to the tip. Near-field antenna action, local strain and heating, doping by hot-carrier injection likely possess different areas of influence inside the sample under study, *i.e.*, affect different volumes of the sample beneath the tip, which is located on or close to the sample surface. As a consequence, a spectrum taken in the presence of the tip (tip-in spectrum) is not simply a near-field spectrum originating from the sample region close to the tip (which is much smaller than the volume corresponding to the laser focus) added to the spectrum originating from the laser focus without the tip being present (tip-out spectrum). Not all differences in the tip-in spectra can necessarily be attributed to LSP excitations. Basically strain and temperature changes introduced by the tip will also affect the far-field response of the sample. As a consequence, a clear distinction between near-field effects and far-field effects is not possible in the presence of the tip and they are difficult to disentangle. This has an influence on the calculation of the enhancement factor, an important parameter in SERS and TERS. The enhancement factor is described as the intensity ratio between SERS/TERS and conventional Raman spectra of a sample. Consequently, an enhancement factor is difficult to define in a reliable manner in case of thin-film samples.

Molybdenum disulfide (MoS_2) is a prominent member of the transition metal dichalcogenides (TMDC). All structural polytypes of MoS_2 crystallize in a characteristic layered structure, where a Mo-atom layer is sandwiched between two S-atom layers.[14] Since adjacent MoS_2 layers are only weakly bound to each other by van der Waals interaction, individual sheets can be separated quite easily. An established method for separating single layers from a natural bulk material is mechanical exfoliation.[15,16] The electronic structure of MoS_2 depends strongly on the number of layers. In particular, its electronic band structure changes from an indirect to a direct semiconductor when reducing bulk material to a single MoS_2 layer. For this reason, single layer MoS_2 exhibits a very strong photoluminescence quantum yield, which decreases with an increasing number of MoS_2 layers.[17] In a typical PL spectrum, two direct transitions (A and B) occur due to the spin-split valence bands (VB) at the K (K′) points.[18] In addition, at least one indirect transition is observed in multilayer MoS_2 samples.[19] Furthermore, since the Raman spectrum of few-layer MoS_2 strongly depends on the number of layers, the positions of the in-plane E_{2g} and the out-of-plane A_{1g} mode can be used to determine the layer thickness of thin sheets.[20–22]

The layer-dependent band structure, the existence of a band gap in the visible range, crystallization in a 2D-layered structure and the associated possibility to exfoliate single and few-layer sheets makes MoS_2 an interesting model system for TERS/TEPL studies. There exists already some theoretical and experimental work on TERS/TEPL on MoS_2.[23–28] However, most experimental studies focus on spatial resolution, especially the resolution of local heterogeneities (such as defects, strain, doping, *etc.*) and are often limited to single MoS_2 layers only. Here, we present results of a systematic investigation of the TERS and TEPL response as function of the number of MoS_2 layers employing the same tip. This study demonstrates clearly that the presence of the tip has an additional impact of the MoS_2 sheets, besides the near-field antenna action. The analysis of experimental findings yields a better understanding of the microscopic mechanisms underlying tip-enhanced optical spectroscopic techniques and their interplay with the different electronic and vibrational structures of MoS_2 samples with a different number of layers. It becomes apparent that the interaction ranges of the different contributions to the TERS signal vary for MoS_2 samples of different thickness.

2 Methods

2.1 Mechanical exfoliation and sample identification

Ultrathin sheets of MoS_2 were obtained by mechanical exfoliation of natural bulk crystals onto heavily p-type doped Si substrates with a 275 nm thick wet-thermal oxide layer (Siegert Wafer GmbH, Aachen, Germany). Single, few and multi-layer MoS_2 samples were identified by optical contrast imaging and the assignment was confirmed by Raman and PL spectroscopy.

2.2 Setup

The Raman and the PL spectra were recorded at room temperature in back-scattering geometry using a Renishaw inVia Raman microscope system combined with a MultiView 2000 (Nanonics Imaging Ltd, Jerusalem, Israel) for the TERS and TEPL measurements. The MultiView 2000 uses normal force tuning fork technology with phase feedback for the distance control between TERS tip and sample. A Nd:YAG laser with an emission wavelength of 532 nm was focused onto the sample with a 50× LD microscope objective (Nikon, NA = 0.45). The laser spot was approximately 2 μm in diameter. Except for the laser-power dependent measurements the laser power was set to 2.48 mW. The scattered light was collected by the same objective and then coupled into a spectrometer, where it was dispersed using a diffraction grating with either 2400 lines per mm or 1800 lines per mm and the resulting spectrum recorded using a charge-coupled device camera (CCD). The 2400 lines per mm grating was used for TERS whereas the 1800 lines per mm grating for the TEPL and the temperature and laser-power dependent measurements. The spectrometer in conjunction with the CCD provided a spectral resolution better than 1.5 cm^{-1}. The acquisition times for the TERS and TEPL spectra were 5 and 10 s per frame, respectively. For the temperature dependent measurement, a custom-made sample stage with an integrated Peltier element was used allowing us to control the substrate temperature in a range of 10 °C to 95 °C. All PL spectra were response-corrected using a calibrated tungsten-halogen lamp (Oriel, spectral range 250–2400 nm) as reference standard. Due to the wide spectral range, a specific measuring mode had to be used for acquiring the PL spectra. In this mode, the full PL spectra are assembled out of CCD frames obtained at different grating positions with a spectral

overlap between adjacent frames corresponding to the width of 10 pixels on the CCD chip. The partial spectra are automatically assembled by the software. The principal component analyses of the far- and near-field Raman and photoluminescence spectra were performed using the corresponding routines of the software package OriginPro.

3 Experimental results and discussion

We have performed TERS and TEPL experiments on several mechanical exfoliated single, few and multi-layer MoS_2 sheets. Fig. 1(a) shows an optical microscope image of a MoS_2 flake, which consists of single-layer (1L), bi-layer (2L), triple-layer (3L) and bulk-like multi-layer (MuL) areas. In a typical TERS/TEPL experiment, two different kinds of spectra are recorded: a tip-in spectrum, where the tip is centred in the focus of the laser beam and a tip-out spectrum taken at the same spot without the impact of the tip. In the latter case, the tip can be retracted of the sample surface by the z-piezo element or it can be completely laterally removed. As schematically illustrated in Fig. 1(b), we decided to use the second approach, whereby the TERS tip is moved manually to the respective parking position outside the laser focus. For the tip-in spectrum, the TERS tip was positioned at that point in the laser spot where the intensity of the recorded spectrum was highest. The results of the TERS/TEPL measurements are shown in Fig. 1(c) and (d), respectively. The Raman spectra show the doubly degenerate E_{2g} and the non-degenerate A_{1g} signals, which correspond to in-plane and out-of-plane phonon modes, respectively.[22] The PL spectra reveal the A and B bands corresponding to the direct band-gap transition at the K-points of the Brillouin zone. For all samples, but 1L MoS_2, we also detect bands due to indirect transitions between the conduction band minima, one occurring along the Λ-direction between Γ- and K-point and the other at the K-point itself, and the highest valence band at the Γ-point.[19,29] All tip-in spectra are significantly

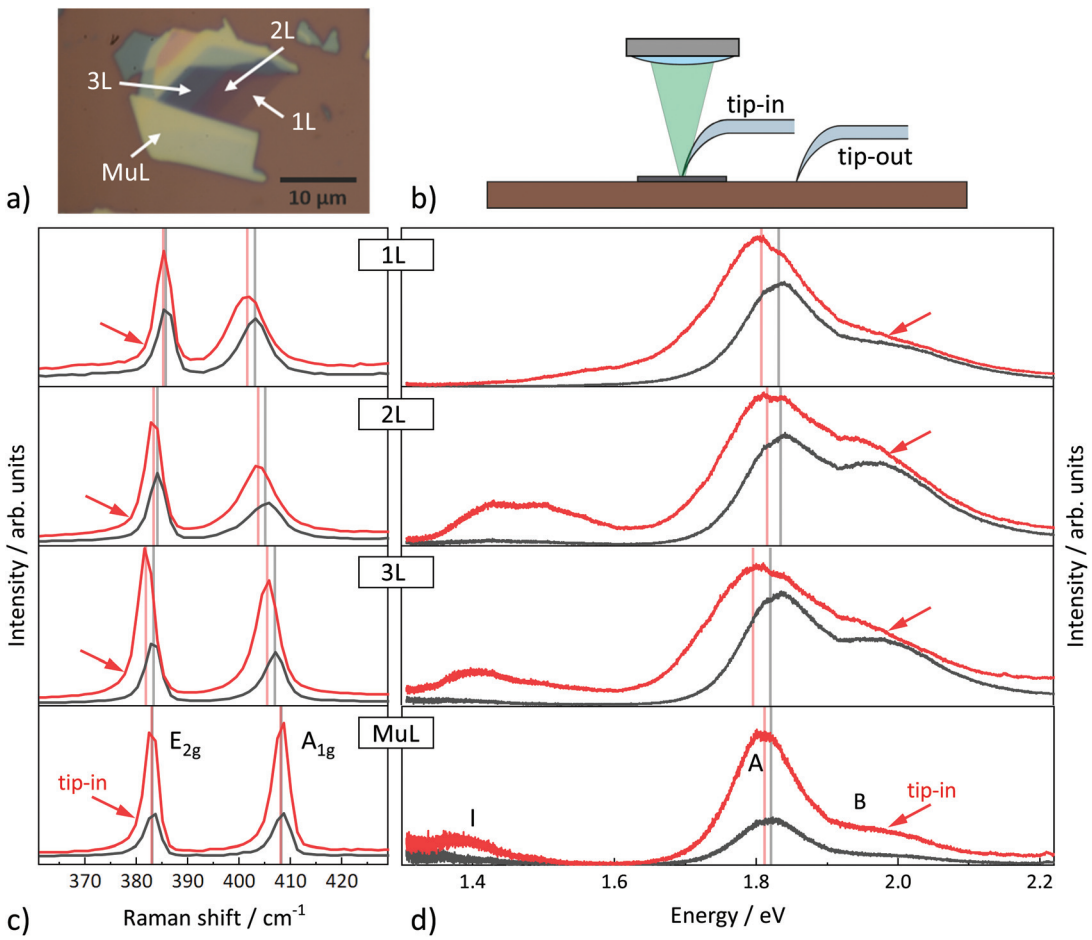

Fig. 1 (a) Optical microscope image of a mechanical exfoliated MoS_2 flake on a Si/SiO_2 substrate. (b) Schematic illustration of the TERS/TEPL-process. (c) and (d) Tip-in (red, additionally marked with an arrow) and tip-out (black) Raman (c) and PL (d) spectra of MoS_2 sheets with a different number of layers. In addition to the red-shift of the direct transitions and the enhancement of the PL signal, there exist a significant change of the spectral shape of the tip-in TEPL spectra. Each pair of tip-in and tip-out spectra is plotted on the same scale. The light black and red lines reflect the positions of the Raman modes and the A transition of the tip-out and tip-in spectra as obtained from the Lorentzian and Gaussian profiles.

enhanced in intensity compared to the corresponding tip-out spectra. Furthermore, the tip-induced intensity enhancement is accompanied by changes of the spectral features in terms of linewidths, positions, and relative intensities. For example, there is a significant red-shift of the features in the tip-in Raman spectra as well as in the direct photoluminescence transitions A and B. This is a clear indication that the effect of the tip on the sample and, thus, on the tip-in Raman spectrum, is more than just the tip's near-field antenna action. Such multifarious changes of the spectra induced by the presence of the tip occur in qualitatively the same manner for all regions probed on the sample, *i.e.*, 1L, 2L, 3L, and bulk-like MoS_2 material.

In what follows, we will examine the differences between the tip-in and the tip-out spectra in more detail and a first analysis of the impact of different external perturbations induced by the tip on the Raman and PL spectra. For this purpose, we performed additional temperature and laser-power dependent measurements of tip-out PL and Raman spectra at positions on the sample corresponding to 1L, 2L and bulk-like MoS_2 material. The spectra are shown in the ESI.† A red-shift of the Raman modes and the direct PL-transitions in the spectra are also observed when the laser intensity or the temperature are increased. Principal component analyses (PCA) were carried out in order to emphasize that the changes in the tip-in spectra are not solely caused by a local increase of laser power or temperature. PCA is a statistical technique that is often used to structure and visualize multidimensional data sets by reducing the information they contain to two or three-dimensional graphs of a few uncorrelated variables, the so called principal components (PCs). The underlying transformation implies a, though minimized, loss of information. However, this deficit is commonly accepted in favour of a better and easier interpretability of the data. In the PCA, n spectra (in our case temperature and laser-power dependent tip-out spectra, TERS/TEPL spectra), each with m spectral positions, can be considered as n single points in an m-dimensional space. Each coordinate axis corresponds to a spectral position and the intensity value of a spectrum at that position defines the coordinate value. In the PCA a new coordinate system is chosen to present the same set of data. For this purpose, the covariance matrix of the spectra in the original coordinates is calculated and the matrix's eigenvalues are derived. All eigenvalues are positive because they correspond to variances and are labelled in descending order, *i.e.* largest variance to smallest variance. The corresponding eigenvectors (PC loadings) point along the directions of the principal axes (PCs) of the new coordinate system. The new coordinates of each spectrum are its PC scores. Typically, the first few PCs (*e.g.*, PC1, PC2, PC3) retain most of the statistical information present in all of the original variables.[30] Resulting 2D graphs, such as plots of PC1 *vs.* PC2 scores of all spectra, highlight the differences between the spectra, since data points of related spectra will cluster together and those of different ones will be spread out.

Corresponding PCA results for 1L and 2L MoS_2 are displayed in Fig. 2. In both cases, two PCA were performed, one for the set of Raman spectra and another one for the set of PL spectra. All spectra were normalized prior to the PCA in order to focus on spectral differences such as relative intensity changes, shifts in position or changes in linewidth. PCA results of the Raman spectra are depicted on the left and those of the PL spectra on the right of Fig. 2. In all graphs, each data point represents one spectrum. Data points in blue correspond to the series of temperature-dependent tip-out spectra and black data points to the series of tip-out spectra where the intensity of the excitation laser was varied. The red data points correspond to tip-in spectra taken at positions on the sample with the corresponding number of MoS_2 layers. The barycenter of the data points corresponding to the tip-in spectra are clearly separated from those of the temperature dependent and the laser-power dependent spectra in the PCA score plots in all four graphs. A clearer delineation of the Raman data points can be achieved when considering pairs of classes only (see, *e.g.*, ref. 31). Results of such analyses of the Raman data of 1L and 2L MoS_2 are discussed in the ESI.† These additional PCA are based on sets of spectra comprising only two classes of spectra, the tip-enhanced series with either all the temperature dependent or all the power dependent spectra. A separation of the data points of the two classes studied is achieved in all cases. Furthermore, the corresponding spectra are correlated with the scores and loadings of the PCA. Based on the results shown in Fig. 2 and the thorough analysis of the PCA results in the ESI,† we can state that a local temperature rise or an increase of the laser power alone or both together cannot explain all the changes of the TERS and direct TEPL spectra observed in case of the 1L and 2L MoS_2. Another microscopic effect must be induced by the tip to explain the experimental observations.

In what follows, we will analyse the spectral changes in more detail and suggest that hot-carrier injection significantly contributes to the differences between tip-in and tip-out spectra. In particular, two features in the tip-in spectra suggest a charge carrier injection from the TERS tip to the MoS_2 sheets. First, there is the significant increase in the indirect band transition in case of few-layer MoS_2 flakes. Fig. 3(a) shows an enlarged view of the indirect band transitions of 2L-MoS_2. Of all investigated MoS_2 sheets, the bilayer shows the largest enhancement and change of the spectral shape in the tip-in PL spectrum recorded in the spectral range of the indirect transitions. Due to the band structure of 2L MoS_2, two indirect band transitions, I_1 ($\Lambda \rightarrow \Gamma$) and I_2 ($K \rightarrow \Gamma$), are possible at room temperature.[19] While the features due to I_1 and I_2 in the tip-out spectrum are hard to distinguish, the higher energy emission peak I_2 is more pronounced in the tip-in spectrum. Furthermore, both peaks are considerably enhanced in the tip-in spectrum compared to the tip-out spectrum. As illustrated schematically in Fig. 3(b), the location of the Fermi level may be modified by the TERS tip and is finally located in the K and Λ valley of the conduction band (CB). As a result, electrons can also accumulate in the higher CB valley and take part in the recombination process of the photoluminescence. In case of 1L MoS_2, the band structure is different as can be seen in

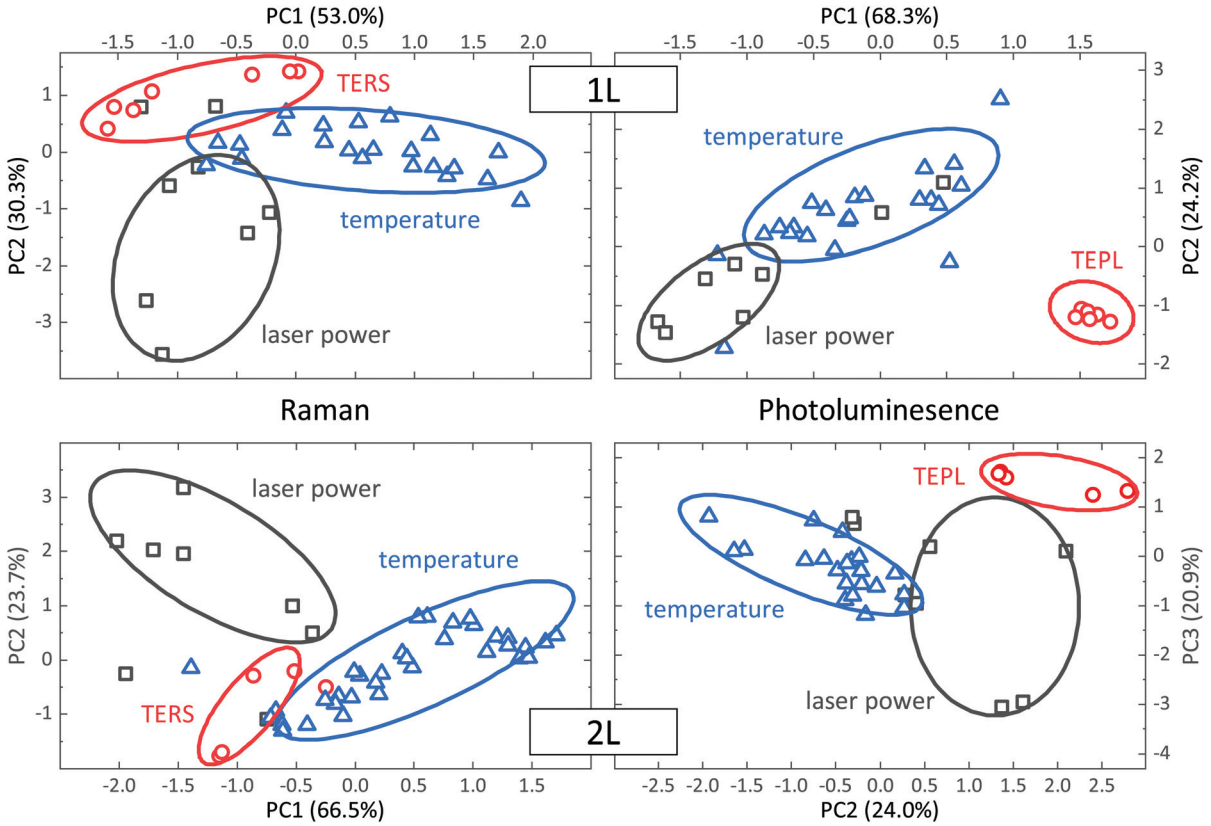

Fig. 2 PCA score plots of 1L and 2L MoS_2 tip-in and tip-out spectra. Raman (left) and direct PL spectra (right) were analysed separately. In both cases the barycenter's of the near-field signals are separated, and so the significant shift and the deviating spectral shape of the TERS/TEPL spectra cannot be solely caused by an increase of temperature or laser power, respectively. All spectra were normalized prior to the PCA. All spectra were collected with an 1800 l mm^{-1} grating.

Fig. 3(b). The CB valley along the Λ-direction is considerably higher in energy than that at K. Furthermore, the VB maxima at Γ and K are very close in energy. Thus, an indirect transition from the CB valley along Λ to the VB maximum at the Γ-point or that at the K-point is unlikely and would be higher in energy than the direct A and B transition. Therefore, no additional PL band occurs between 1.4 and 1.5 eV in the tip-in spectrum of 1L MoS_2.

A second point in favour of an electron doping of the MoS_2 is the broadening of the A_{1g} mode of the monolayer by about 2 cm^{-1} in the near-field spectra. As Chakraborty *et al.* demonstrated in their *in situ* Raman experiments from a 1L MoS_2 top-gated field-effect transistor, the A_{1g} mode shows a strong doping dependence. The n-doping leads to a reduction of the phonon frequency and a broadening of the linewidth of the A_{1g} mode. This can be explained by the strong electron–phonon coupling between the A_{1g} mode and the injected carriers.[8]

The behaviour of the A_{1g} mode and the indirect band transition of the PL in the near-field spectra clearly indicate an increase of the carrier concentration in the MoS_2. This seems unusual in view of the higher work function of Au compared to MoS_2. In particular, as it was recently reported that 1L MoS_2 can be p-doped by an Au-tip, *i.e.*, electrons are extracted in contact with the Au-tip.[24] Apart from a different choice of substrate and a different measurement setup in those experiments, the main difference to our work is the design of the tip used. Su *et al.* used Au and Ag coated Si tips for their contact TEPL measurements. In that case, the impinging laser wavelength of 532 nm was not in resonance with the LSP of the Au tip. Instead, we used commercially acquired glass fibre TERS-tips (Nanonics Imaging Ltd, Jerusalem, Israel) with embedded Au nanoparticles at the tip apex. The LSPs of the Au nanoparticles of our tips are resonant with 532 nm excitation due to the smaller size of the nanoparticles. This other experimental constellation leads to a charge transfer of so-called hot-electrons from the TERS tip to the adjacent MoS_2 layer, as the electrons can acquire enough energy to overcome the Schottky barrier between Au and MoS_2. Similar hot-electron doping has already been demonstrated in SERS experiments with various Au nanoparticles on monolayer MoS_2 and graphene. In both cases, the plasmon-induced n-doping of the 2D-material influenced the Raman spectra of the 2D material taken in the vicinity of the Au particles significantly. In the presence of Au nanoparticles, Weinhold *et al.* observed a blue-shift of the G-mode of graphene, which can be explained by electron–phonon coupling between graphene phonons at the Γ-point and the transferred electrons forming a free-carrier plasma.[32] In 1L

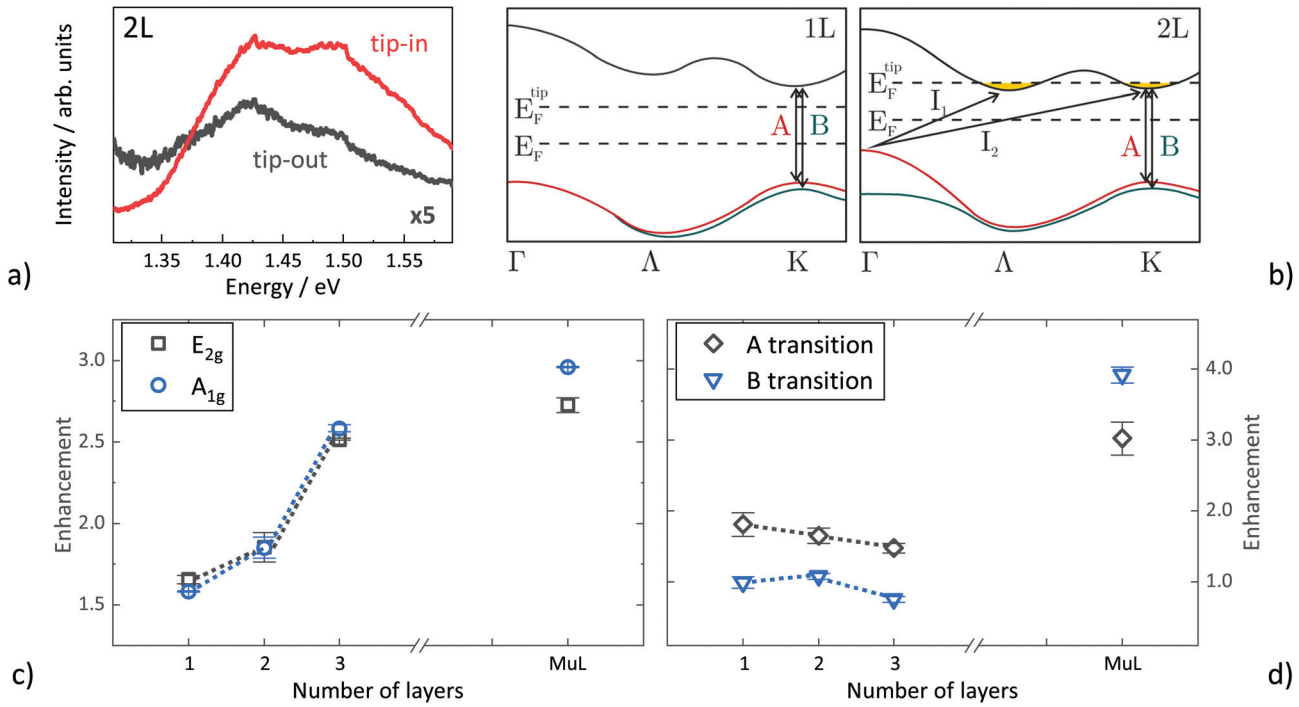

Fig. 3 (a) Closer look of the indirect bandgap transition of a measured bilayer MoS_2 TEPL spectra. Especially the higher energy emission peak (I_2) of the tip-in spectrum is significantly enhanced compared to the tip-out spectrum. The tip-out spectrum is multiplied by a factor of 5 and both spectra are smoothed, for clarity. (b) Schematic, reduced illustration of the electronic band structure of mono- (1L) and bilayer (2L) MoS_2. The enhancement of the indirect band gap, especially of the higher energy emission peak, can be correlated with a charge transfer (n-doping of the MoS_2) and a corresponding Fermi level tuning by the TERS-tip. Band structures reproduced from ref. 29. (c) and (d) Enhancement of the near-field spectra as a function of the layer number for the Raman modes (c) and the direct PL transitions (d).

MoS_2, the additional hot-electron doping can even destabilize the crystal lattice and introduces a reversible 2H-to-1T phase transition, *i.e.* strain.[33] Accordingly, not only the material of the tip but also the tip's microstructure or design is decisive for a possible charge transfer at a fixed excitation wavelength, *i.e.* alters the magnitude of different tip-induced microscopic effects affecting the Raman and PL spectrum.

We will now turn to the analysis of the tip-induced enhancement of the two direct transitions A and B in the PL spectra as well as of the two Raman modes in dependence on the number of MoS_2 layers. For this purpose, we fitted the two Raman modes and the two direct PL transitions by two Lorentzian and two Gaussian profiles, respectively. In addition, the PL spectra were background corrected prior to the fitting. To quantify the enhancement of a spectral feature introduced by the tip, the ratio of the areas of the peaks given by the fitted lineshapes of the tip-in and tip-out spectrum were calculated. Enhancement factors determined in this fashion are considerably lower than those commonly reported, because we make no attempt to estimate the effective enhancement by multiplying an additional weighting factor arising from the ratio of the comparatively large volume characteristic for far-field effects and the very small volume characteristic for near-field effects.[34–36] Correcting for this volume ratio yields enhancement factors, that are several orders of magnitude higher. As pointed out in the introduction, such a definition of an effective enhancement is only justified, if the differences between tip-in and tip-out spectrum almost solely arise due to the antenna action of the tip, which is not the case in our experiments, as demonstrated above. Fig. 3(c) and (d) show that the Raman and die PL signals are differently enhanced. The clearest differences can be observed for the few-layer samples. In TERS, both Raman modes are enhanced by a similar factor in spectra taken at positions with the same number of MoS_2 layers. A clear trend is observed as a function of MoS_2 layer number. The enhancement factor increases stepwise from 1L to MuL. This trend is surprising and counterintuitive, since the electromagnetic enhancement of SERS and TERS due to the antenna action should be of short-range as a near-field effect.[2,37] Thus, one would expect that the near-field contribution in the tip-in spectrum in relation to the tip-out spectrum should be largest for the single layer and should decrease with increasing number of layers, *i.e.*, leading to a decrease of the enhancement factor with increasing number of layers, in a homogeneous material. This suggests that the changes of the electronic and phononic structure with the number of MoS_2 layers as well as the underlying substrate may also affect the magnitude of the enhancement observed. The impact of two different Si/SiO_2 substrates on the enhancement factors was investigated layer-dependent for three different MoS_2 flakes and is discussed in the ESI.† The trend as a function of MoS_2 layer number as well as the magnitude of the

enhancement are significantly affected by the structural composition of the oxide interface. Furthermore, different nominally similar TERS tips were also employed. However, the variation in the commercially purchased tips due to manufacturing seems to play a minor role only.

An interesting trend can also be observed for the TEPL enhancement. In the few layer sheets only a significant enhancement of the A-transition is observed. Probably an increase of the B-signal is suppressed by VB–VB relaxation of holes at the K-point. In case of TEPL, the largest enhancement factor occurs for MuL MoS_2, with an even more pronounced change of enhancement from 3L to MuL MoS_2 than in TERS. However, it should be noted that temperature effects may play a significant role here. Tongay *et al.* have shown that the intensities of the PL-signals decrease significantly with increasing temperature other than the Raman signals.[10] Local heating by the tip, thus, will cause a decrease in PL intensity counteracting the enhancement effect of the antenna action. In particular, few-layer MoS_2 sheets should be more affected as the thermal conductivity of the underlying SiO_2 substrate is low and thus heat dissipation is slower than in case of MuL MoS_2.

Fig. 4(a) shows the positions of the two Raman-active modes and the direct PL transitions derived by fitting the tip-in and tip-out spectra, results plotted in red and black, respectively. The positions of the two Raman modes in the tip-out spectra reveal the anticipated behaviour known from literature. The E_{2g} mode exhibits a red-shift with increasing number of layers, whereas the A_{1g} mode a blue-shift.[20,22] Virtually the same behaviour is observed for the positions of the Raman modes extracted from the tip-in spectra, but with a red-shift of both modes. There is one exception, *i.e.*, the positions of both Raman modes in the tip-in and tip-out spectra of MuL MoS_2 agree within the experimental uncertainty. The observed behaviour is in accordance with a local heating introduced by the tip, which leads to the red-shift of both Raman modes for 1L, 2L, and 3L MoS_2, but a negligible shift for the modes of MuL MoS_2 as the local heating is less pronounced due to a better heat dissipation. Thus, the behaviour of the Raman mode positions corroborates the interpretation of the results of the PL enhancement.

The absolute value of the change in Raman shift introduced by the tip is displayed for both Raman modes in Fig. 4(c). The change in position of the A_{1g} mode of approx. 1.5 cm^{-1} is almost constant for 1L, 2L, and 3L MoS_2, but zero for MuL MoS_2. In contrast, the change in position of the E_{2g} mode increases from 0.5 cm^{-1} for 1L to 1.5 cm^{-1} for 3L MoS_2 prior to dropping to zero again for MuL MoS_2. The change of position of the A_{1g} is likely due to a combination of temperature increase as well as n-doping by the tip. Whereas the layer-dependent behaviour of E_{2g} is probably due to a combination of local temperature effects and strain. The E_{2g} mode position in MoS_2 is very sensitive to strain, whereas the position of the

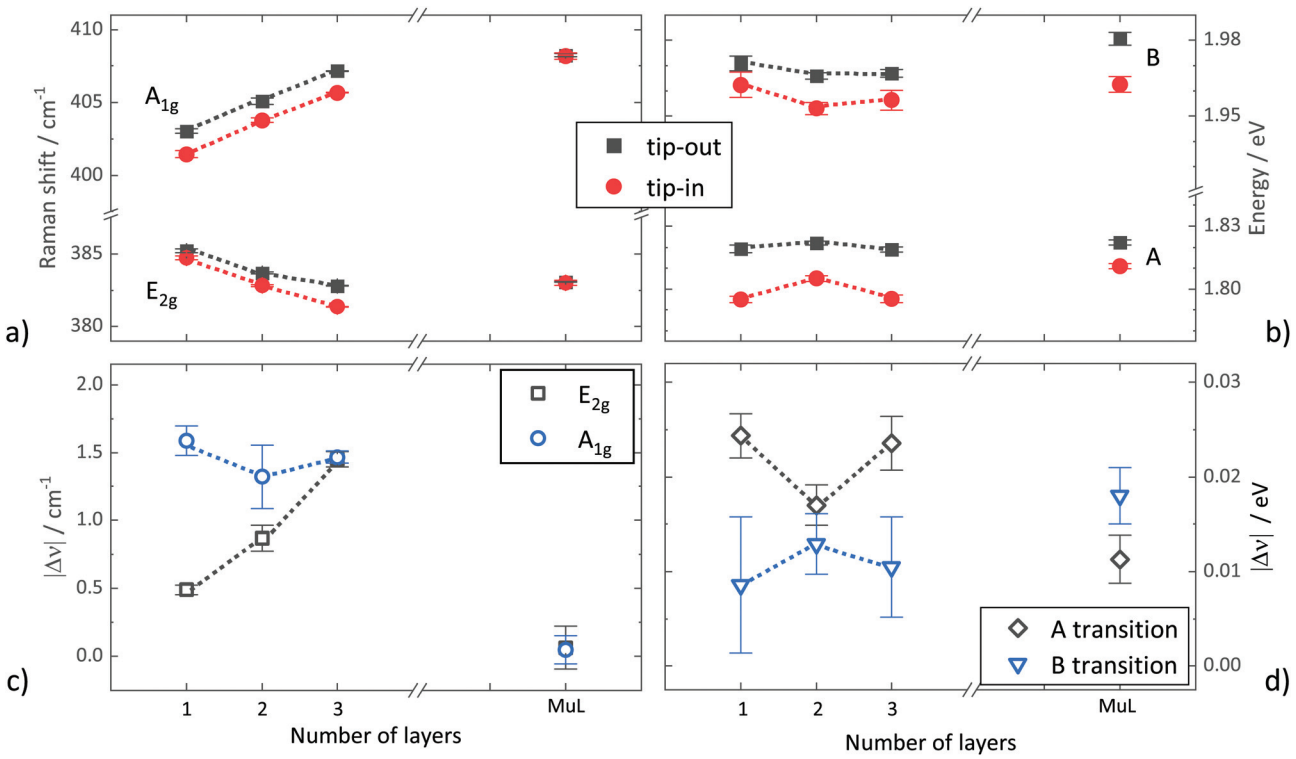

Fig. 4 Layer-dependent influence of the TERS/TEPL effect on the position of the Raman modes (left) and the direct PL transitions (right). (a) and (b) Under the impact of the tip, the two Raman-active modes and the direct PL transitions exhibit a red-shift. (c) and (d) Absolute shift of the two Raman modes and the direct PL transitions against the number of MoS_2 layers. In contrast to the A_{1g} mode, the E_{2g} shows a clear layer-dependence. This can be explained by strain effects in the MoS_2 sheets released by the tip.

A_{1g} mode is hardly influenced by strain.[12,13] Strain may be introduced by the tip either mechanically or indirectly by local heating of the surface underneath or hot-carrier injection. The fact that no change of position of the two Raman-active modes is found for MuL MoS_2 reflects that local effects such as strain, temperature and doping have less impact for two reasons. Firstly, dissipation of heat and carriers is facilitated in the more three-dimensional case and, secondly, the sample volume within the laser spot increases with increasing MoS_2 thickness yielding a larger fraction of the probed volume, which contributes to Raman scattering and is unaffected by the tip.

The positions of the two direct PL bands corresponding to the direct A and B transitions exhibit only a slight dependence on MoS_2 layer number as can be seen in Fig. 4(b), but a general red-shift of the PL features in the tip-in spectra is confirmed. The differences of the energy positions of both direct PL bands in the tip-out and tip-in spectra are given in Fig. 4(d). No clear trend is revealed. The PL energy difference for the A transition is larger than for the B transition for few layer MoS_2, *i.e.*, 1L to 3L, for MuL MoS_2 the situation is reversed. From 1L to 2L MoS_2, the PL energy difference decreases for the A transition, whereas that of the B transition exhibits a slight increase. The situation is opposite again going from 2L to 3L MoS_2. The overall situation is not as clear as in case of the Raman modes. Nevertheless, the position of the PL band of the stronger A band can be reliably fitted, thus, its trend as a function of MoS_2 layer number has to be taken seriously. The contributions of local temperature, strain and hot-carrier injection are difficult to discern. Furthermore, the variation of the electronic structure of MoS_2 with the number of layers, in particular, the transformation from a direct bandgap semiconductor in case of 1L MoS_2 to an indirect bandgap semiconductor in case of 2L MoS_2 will influence the trends observed at least in part.

4 Conclusions

Tip-enhancement effects in Raman and photoluminescence spectra of spatially extended samples such as 2D materials or thin films differ considerably from those in spectra of spatially localized entities such as molecules. The reason is that the tip in case of extended samples introduces not only near-field effects due to antenna action, but also far-field effects. Local heating and local strain may arise at the tip position or hot-carriers may be injected from the metal tip into the sample. These effects, though locally introduced by the tip, may extend further into the sample. The strain field will have a certain spatial extension and heat as well as carriers will diffuse into the sample with different diffusion lengths causing far-field contributions in the spectra. In consequence, the spectra not only vary in intensity, but also change in spectral appearance, *i.e.*, peak positions the linewidth of signals varies, relative intensities between spectral features vary, *etc*. In essence, near-field and far-field effects cannot be separated in tip-spectra as the far-field contributions vary throughout the laser spot and differ from those in the tip-out spectra. One side effect is that the commonly used definition of an enhancement factor, originally introduced in studies of molecules, cannot be applied as it is based on the analysis of the intensity changes between tip-in and tip-out spectra and explicitly assumes that the spectral shape does not change. From a material's perspective, it is clear that the tip-induced far-field contributions to the Raman or PL spectra will originate from sample areas of different extensions, *i.e.*, the areas of influence differ as the diffusion lengths of carriers and heat within the sample are not the same and also differ from the characteristic relaxation length of a local strain field. Our experiments also clearly show that the magnitude of the near-field and far-field effects varies with increasing number of MoS_2 layers. There are two main reasons. The first is the significant variation of the phonon and band structure with the number of MoS_2 layers, *i.e.*, due to variation of the intrinsic properties of samples under study with layer thickness. The second reason is due to the variation of external parameters. The dimensionality of the sample changes when going from a single MoS_2 layer to thicker bulk-like MoS_2 affecting heat and carrier diffusion as well as field enhancement. In addition, the coupling of the sample to the environment cannot be neglected. It comprises the choice of substrate as much as the choice of the kind of TERS tip. The analysis of TERS and TEPL is very complex and requires additional carefully conducted studies in order to comprehensively understand the underlying microscopic processes and thus to fully explore TERS and TEPL as non-invasive analytical tools. Semiconducting MoS_2 as well as other 2D materials where samples with a defined number of layers are available are ideal model systems for such studies despite possible variations of the phonon and band structure.

Data availability

The Raman and PL spectra that support the findings of this study are openly available in JLUpub at http://dx.doi.org/10.22029/jlupub-188.

Conflicts of interest

There are no conflicts to declare.

Acknowledgements

Funding by the EU in the framework of the ERDF scheme of the state of Hesse in gratefully acknowledged. S. C. also acknowledges financial support from the German Science Foundation through SFB1083 (Project-ID 223848855) and the Heisenberg Programme (CH660/8).

References

1 *Surface-Enhanced Raman Scattering*, ed. K. Kneipp, M. Moskovits and H. Kneipp, Springer-Verlag, Berlin Heidelberg, 2006, p. 466.
2 K. F. Gibson and S. G. Kazarian, *Encyclopedia of Analytical Chemistry*, John Wiley & Sons, Ltd, Chichester, UK, 2014, vol. 88, pp. 1–30.
3 K. A. Willets and R. P. Van Duyne, *Annu. Rev. Phys. Chem.*, 2007, **58**, 267–297.
4 S. A. Maier, *Plasmonics: Fundamentals and Applications*, Springer, New York, 1st edn, 2007, p. 224.
5 K. Wu, J. Chen, J. R. Mcbride and T. Lian, *Science*, 2015, **349**, 632–635.
6 M. Zhang, R. Wang, Z. Zhu, J. Wang and Q. Tian, *J. Opt.*, 2013, **15**, 055006.
7 R. Zhang, Y. Zhang, Z. C. Dong, S. Jiang, C. Zhang, L. G. Chen, L. Zhang, Y. Liao, J. Aizpurua, Y. Luo, J. L. Yang and J. G. Hou, *Nature*, 2013, **498**, 82–86.
8 B. Chakraborty, A. Bera, D. V. Muthu, S. Bhowmick, U. V. Waghmare and A. K. Sood, *Phys. Rev. B: Condens. Matter Mater. Phys.*, 2012, **85**, 2–5.
9 P. J. Ko, A. Abderrahmane, T. V. Thu, D. Ortega, T. Takamura and A. Sandhu, *J. Nanosci. Nanotechnol.*, 2015, **15**, 6843–6846.
10 S. Tongay, J. Zhou, C. Ataca, K. Lo, T. S. Matthews, J. Li, J. C. Grossman and J. Wu, *Nano Lett.*, 2012, **12**, 5576–5580.
11 R. Yan, J. R. Simpson, S. Bertolazzi, J. Brivio, M. Watson, X. Wu, A. Kis, T. Luo, A. R. Hight Walker and H. G. Xing, *ACS Nano*, 2014, **8**, 986–993.
12 C. Rice, R. J. Young, R. Zan, U. Bangert, D. Wolverson, T. Georgiou, R. Jalil and K. S. Novoselov, *Phys. Rev. B: Condens. Matter Mater. Phys.*, 2013, **87**, 1–5.
13 H. J. Conley, B. Wang, J. I. Ziegler, R. F. Haglund, S. T. Pantelides and K. I. Bolotin, *Nano Lett.*, 2013, **13**, 3626–3630.
14 P. A. Bertrand, *Phys. Rev. B: Condens. Matter Mater. Phys.*, 1991, **44**, 5745–5749.
15 K. Novoselov, A. K. Geim, S. V. Morozov, D. Jiang, Y. Zhang, S. V. Dubonos, I. V. Grigorieva and A. A. Firsov, *Science*, 2004, **306**, 666–669.
16 Y. Huang, E. Sutter, N. N. Shi, J. Zheng, T. Yang, D. Englund, H. J. Gao and P. Sutter, *ACS Nano*, 2015, **9**, 10612–10620.
17 A. Splendiani, L. Sun, Y. Zhang, T. Li, J. Kim, C. Y. Chim, G. Galli and F. Wang, *Nano Lett.*, 2010, **10**, 1271–1275.
18 K. F. Mak, C. Lee, J. Hone, J. Shan and T. F. Heinz, *Phys. Rev. Lett.*, 2010, **105**, 2–5.
19 W. Zhao, R. M. Ribeiro, M. Toh, A. Carvalho, C. Kloc, A. H. Castro Neto and G. Eda, *Nano Lett.*, 2013, **13**, 5627–5634.
20 C. Lee, H. Yan, L. E. Brus, T. F. Heinz, J. Hone and S. Ryu, *ACS Nano*, 2010, **4**, 2695–2700.
21 H. Li, Q. Zhang, C. C. R. Yap, B. K. Tay, T. H. T. Edwin, A. Olivier and D. Baillargeat, *Adv. Funct. Mater.*, 2012, **22**, 1385–1390.
22 A. Molina-Sánchez and L. Wirtz, *Phys. Rev. B: Condens. Matter Mater. Phys.*, 2011, **84**, 1–8.
23 L. Meng and M. Sun, *Photonics Res.*, 2017, **5**, 745.
24 W. Su, N. Kumar, S. Mignuzzi, J. Crain and D. Roy, *Nanoscale*, 2016, **8**, 10564–10569.
25 D. V. Voronine, G. Lu, D. Zhu and A. Krayev, *IEEE J. Sel. Top. Quantum Electron.*, 2017, **23**, 138–143.
26 M. Rahaman, R. D. Rodriguez, G. Plechinger, S. Moras, C. Schüller, T. Korn and D. R. Zahn, *Nano Lett.*, 2017, **17**, 6027–6033.
27 A. G. Milekhin, M. Rahaman, E. E. Rodyakina, A. V. Latyshev, V. M. Dzhagan and D. R. Zahn, *Nanoscale*, 2018, **10**, 2755–2763.
28 A. Rodriguez, T. Verhagen, M. Kalbac, J. Vejpravova and O. Frank, *Phys. Status Solidi RRL*, 2019, **13**, 1–7.
29 T. Brumme, M. Calandra and F. Mauri, *Phys. Rev. B: Condens. Matter Mater. Phys.*, 2015, **91**, 1–19.
30 I. T. Jollife and J. Cadima, *Philos. Trans. R. Soc., A*, 2016, **374**, 20150202.
31 L. Chen, N. C. Carpita, W. D. Reiter, R. H. Wilson, C. Jeffries and M. C. McCann, *Plant J.*, 1998, **16**, 385–392.
32 M. Weinhold, S. Chatterjee and P. J. Klar, *Commun. Phys.*, 2019, **2**, 1–10.
33 Y. Kang, S. Najmaei, Z. Liu, Y. Bao, Y. Wang, X. Zhu, N. J. Halas, P. Nordlander, P. M. Ajayan, J. Lou and Z. Fang, *Adv. Mater.*, 2014, **26**, 6467–6471.
34 N. Hayazawa, Y. Inouye, Z. Sekkat and S. Kawata, *J. Chem. Phys.*, 2002, **117**, 1296–1301.
35 D. Mehtani, N. Lee, R. D. Hartschuh, A. Kisliuk, M. D. Foster, A. P. Sokolov and J. F. Maguire, *J. Raman Spectrosc.*, 2005, **36**, 1068–1075.
36 N. Jiang, E. T. Foley, J. M. Klingsporn, M. D. Sonntag, N. A. Valley, J. A. Dieringer, T. Seideman, G. C. Schatz, M. C. Hersam and R. P. Van Duyne, *Nano Lett.*, 2012, **12**, 5061–5067.
37 P. K. Jain, W. Huang and M. A. El-Sayed, *Nano Lett.*, 2007, **7**, 2080–2088.